Extracting Cardiac Myofiber Orientations from High Frequency Ultrasound Images

Xulei Qin [1], Zhibin Cong [1], Rong Jiang [2], Ming Shen [2],
Mary B. Wagner [2], Paul Kishbom [3], Baowei Fei [1,4, 5 *]

[1]*Department of Radiology and Imaging Sciences, Emory University, Atlanta, GA*
[2]*Department of Pediatrics, Emory University School of Medicine, Atlanta, GA*
[3]*Department of Surgery, Emory University School of Medicine, Atlanta, GA*
[4]*Department of Biomedical Engineering, Emory University and Georgia Institute of Technology*
[5]*Department of Mathematics & Computer Science, Emory University, Atlanta, GA*
*Corresponding author: bfei@emory.edu; Website: www.feilab.org

ABSTRACT

Cardiac myofiber plays an important role in stress mechanism during heart beating periods. The orientation of myofibers decides the effects of the stress distribution and the whole heart deformation. It is important to image and quantitatively extract these orientations for understanding the cardiac physiological and pathological mechanism and for diagnosis of chronic diseases. Ultrasound has been wildly used in cardiac diagnosis because of its ability of performing dynamic and noninvasive imaging and because of its low cost. An extraction method is proposed to automatically detect the cardiac myofiber orientations from high frequency ultrasound images. First, heart walls containing myofibers are imaged by B-mode high frequency (>20 MHz) ultrasound imaging. Second, myofiber orientations are extracted from ultrasound images using the proposed method that combines a nonlinear anisotropic diffusion filter, Canny edge detector, Hough transform, and K-means clustering. This method is validated by the results of ultrasound data from phantoms and pig hearts.

Keywords: Cardiac myofiber orientation, High frequency ultrasound imaging, Nonlinear anisotropic diffusion filter, Orientation extraction, Heart, Denoising,

1. INTRODUCTION

During the heart beating process, cardiac myofibers are the basic force units to make the heart diastolic or systolic, and to pump blood into the circulation [1]. The orientation of cardiac myofibers determines the stress distribution within the cardiac walls, and also determines the deformation of the whole heart during beating periods, hence will affect the heart functions, such as ejection fraction. Therefore, extracting cardiac myofiber orientations has the potential not only for quantitative analysis of heart functions but also for diagnosis and treatment of chronic cardiovascular diseases. However, the distribution of cardiac myofiber orientations is complex in the heart and is difficult to image and to quantify. There were previous research efforts in this area by using the histology analysis methods [2, 3]. Currently, magnetic resonance diffusion tensor imaging (MR-DTI) is used as a popular method to extract myocardial fiber orientation [4-6]. MR-DTI can measure the diffusion tensor for water in biological tissues. Its main advantage is that three-dimensional myofiber direction vectors can be extracted as the principal direction of the diffusion tensor. However, this process is time consuming and usually requires the subjects to hold their breath to avoid the unnecessary motion during the whole imaging experiment process. Thus, the resolution of MR-DTI images will be decreased during the experiments *in vivo*. In contrast, ultrasound imaging that has been widely used in cardiac diagnosis can be done in real time and is cost effective. It has the potential to dynamically image cardiac myofiber orientation in the beating heart. Therefore, researchers have attempted to extract the relationships between cardiac myofiber orientations and ultrasound anisotropic imaging characteristics [7-9]. Recently, Lee et al. used a shear wave imaging method to obtain the cardiac myofiber orientations in vivo and compared these findings with MR-DTI results [10, 11].
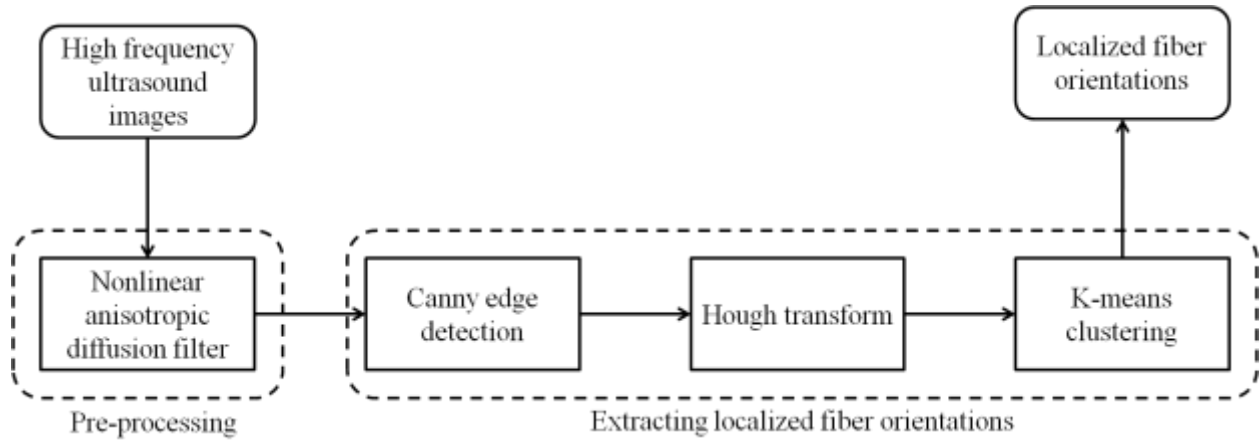
Figure 1. Flowchart for extracting myocardial fiber orientations from high frequency ultrasound images.

Being different from the indirect methods mentioned above, we propose a method that directly extracts myofiber orientations from high frequency (25-40 MHz) ultrasound images. We initially test the feasibility of high frequency ultrasound to directly image the cardiac myofiber structures. Then an extraction method is proposed to extract the orientations of these fibers from the high frequency ultrasound images with many speckle noises. The proposed method contains a nonlinear anisotropic diffusion filter to decrease the speckle noises in ultrasound images, a Canny edge detector to detect the myofiber edges, a Hough transform to extract the orientations based on the detected edges, and finally a K-means clustering classification method to set a localized orientation map by classify all fibers into different localized groups.

2. METHODS

Before the cardiac myofiber extracting approach, 2D images of pig heart tissues were acquired using a B-mode high frequency ultrasound system (Vevo 2100, VisualSonics, Toronto, Ontario, Canada). Linear ultrasound probes were used to image the pig heart walls. The myofiber structures are shown as bright regions in Figure 4. In order to extract the orientations from the experimental data, a two-step approach is designed and the flowchart of the method is shown in Figure 1.

2.1 Denoising

The speckle noise level in high frequency ultrasound images is higher than that of general ultrasound images, as shown in Figure 4(a). These noises will heavily increase the difficulty to extract myofiber structures. Therefore, it is necessary to first decrease these noises before any fiber orientation extraction. In order to decrease the speckle noise effect, a nonlinear anisotropic diffusion filter (NLADF) [12-14] is used to denoise the ultrasound images before the fiber orientation extraction step. The filtering method is based on the diffusion equation framework by considering anisotropic diffusion coefficient parameters. Its equation can be written as [12]:

$$I(\bar{x},t)_t = div\ (c(\bar{x},t)\cdot\nabla I(\bar{x},t)),\ t\geq 0\ , \tag{1}$$

Here, I is the intensity at the 2D space location $\bar{x}$, t is the diffusion time and represents iteration steps , ∇ is the gradient operator in the space domain, and c is the diffusion coefficient decided by both space and time domain. c is defined here as:

$$c(\bar{x},t) = \cfrac{1}{1+(\cfrac{\left\|\nabla I(\bar{x},t)\right\|}{K})^2} \quad , \tag{2}$$

Where K is a constant value. Its 2D discrete implementation at point (i, j) can be represented as following:

$$\begin{aligned} I_{i,j}(t + \Delta t) &\approx I_{i,j}(t) + \Delta t * \frac{\partial}{\partial t} I_{i,j}(t) \\ &= I_{i,j}(t) + \Delta t * (\phi_{i,j}^{+x} - \phi_{i,j}^{-x} + \phi_{i,j}^{+y} - \phi_{i,j}^{-y}) \end{aligned} \quad , \tag{3}$$

Where Δt is the iteration step, and ϕ is the four-direction calculator around center point (i, j) :

$$\phi_{i,j}^{+x} = c_{i+\frac{1}{2},j}(t) * (I_{i+1,j}(t) - I_{i,j}(t))$$

$$\phi_{i,j}^{-x} = c_{i-\frac{1}{2},j}(t) * (I_{i,j}(t) - I_{i-1,j}(t))$$

$$\phi_{i,j}^{+y} = c_{i,j+\frac{1}{2}}(t) * (I_{i,j+1}(t) - I_{i,j}(t)) \quad , \tag{4}$$

$$\phi_{i,j}^{-y} = c_{i,j+\frac{1}{2}}(t) * (I_{i,j-1}(t) - I_{i,j}(t))$$

This filter has the advantage of smoothing noises without removing the significant parts of the image content, typically edges, lines or other details, which are important for the myofiber extraction method. The NLADF is suitable for the purpose of decreasing the speckle noises but keeping the main edge information in ultrasound images.

2.2 Localized myofiber orientation extraction

After decreasing speckle noises, a Canny edge detector is then applied to detect the myofiber edges from the pre-processed ultrasound images. This edge detector is useful for myofiber edge detection from ultrasound images because even after decreasing speckle noises, there are fake blur regions in the images. Although the myofiber edges can be detected by the Canny detector, they just show the myofiber locations in the images rather than the direction of the myofiber distribution. Thus, a Hough transform is introduced to extract the myofiber directions [15]. The transform detects imperfect instances of objects within a certain class of shapes such as lines, circles or ellipses. Because myofiber is similar to the thread shape whose longest shape distance indicates its corresponding direction, Hough transform is able to extract the myofiber directions from the detected edges according to a line shape class.

However, Hough transform for direct lines usually produces more than one line for each fiber edge, which means more than one orientation in each localized region. Therefore, a K-means clustering is applied to classify the detected fiber directions into a localized orientation group [14, 16, 17]. Given a set of data ($\bar{x}_1$, $\bar{x}_2$, $\bar{x}_3$, ..., $\bar{x}_n$), where each is a 2D middle point of the detected fiber direction line. The k-means clustering method generally minimizes an defined objective function to classify the whole data set into k classes ($k \leq n$) $\bar{C}$ = { C_1, C_2, ..., C_n }, which is represented as followed [18]:

$$\arg_C \min(\sum_{i=1}^{k} \sum_{x_j \in C_i} \left\| \bar{x}_j - \bar{\mu}_i \right\|^2) , \tag{5}$$

where $\bar{\mu}_i$ is the mean value of points in C_i. Here the class number k is a given number.

Finally, the localized orientations of myofibers are extracted from the high frequency ultrasound images into different localized regions.

2.3 Evaluation

Quantitative performance assessment of the method was conducted by comparing the results with the corresponding manual results. Manual methods are often used as the gold standard for evaluation of classification and segmentation [19-26]. In this study, both mean absolute distance (MAD) and the Hausdorff distance (HD) are used as the performance assessment metrics. Suppose A and B are both edges of automatic and manual results, respectively; and they are represented by point sets: $A = \{a_1, a_2, ..a_m\}$ and $B = \{b_1, b_2, ..b_n\}$, MAD and HD are defined as following:

$$MAD(A,B) = \frac{1}{2}\left\{\frac{1}{m}\sum_{i=1}^{m} d(a_i, B) + \frac{1}{n}\sum_{j=1}^{n} d(b_i, A)\right\}, \tag{6}$$

$$HD(A,B) = \max\left\{\max_i\{d(a_i, B)\}, \max_j\{d(b_j, A)\}\right\}, \tag{7}$$

where $d(a_i, B) = \min_j \|b_j - a_i\|$. MAD is a global measurement of both edges matching. HD is a similarity measure for their locals.

2.4 Experimental design

In order to acquire the high frequency ultrasound images of cardiac myofibers, 5 pig hearts were dissected and then cut into several pieces from both left ventricle and right ventricle. Then these pieces were imaged by placing high frequency linear probes on them *via* gels as medium. The central frequencies of the ultrasound probes were 25 MHz and 40 MHz. After imaging experiments, all tissues are stained and their images are digitized in order to detect the actual fiber orientations, as shown in Figure 4.

Meanwhile, two phantoms were set up by placing threads into a water container: one phantom with parallel threads and the other with crossed threads. High frequency ultrasound probes were placed in the water to image these phantoms in order to validate the accuracy of this proposed method.

3. RESULTS

3.1 Phantom validation results

First, the edge detection accuracy of the proposed method was evaluated by two different phantoms. Figure 2(a) and 3(a) show the images of two phantoms with parallel and crossed threads imaged by the 40-MHz probe. The automatic edge detection results were compared with the corresponding gold standards. MAD and HD results of both phantoms are shown in Table 1. Both MAD results are less than 0.1 mm and the maximum HDs are less than 0.4 mm. The error is mainly caused by the artifacts in the region where the threads crossed. The edges extracted by the proposed method and manual results are shown in Figure 2(d) for the parallel thread phantom and Figure 3(d) for the crossed thread phantom.

Table 1. Evaluations of the edge detection method in phantoms

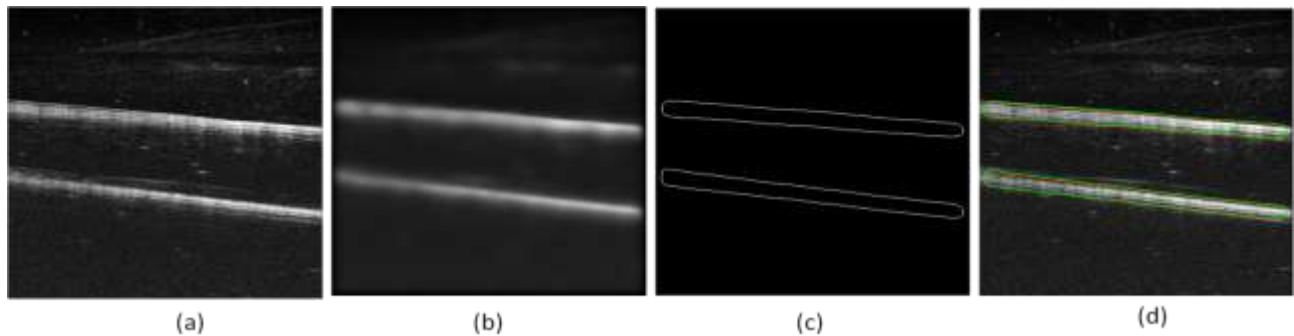| Phantoms	MAD (mm)	HD(mm)
Parallel threads	0.092 ± 0.009	0.26 ± 0.06
Cross threads	0.070 ± 0.011	0.38 ± 0.10

Figure 2. The processed results of the phantom with two parallel threads. (a) The ultrasound image. (b) The result of NLADF. (c) The edge detection result. (d) The detected edges (shown in green) are very close to its corresponding gold standard (shown in red).
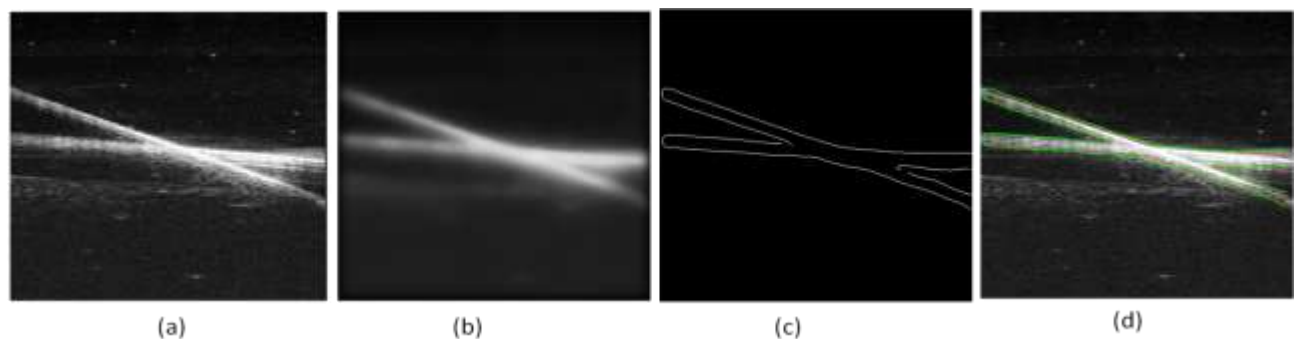

Figure 3. The processed results of the phantom with two crossed threads. (a) The ultrasound image. (b) The result of NLADF. (c) The edge detection result. (d) The detected edges (shown in green) are close to its corresponding gold standard (shown in red).

3.2 Cardiac myofiber extracted orientations

Cardiac myocytes are grouped as myofibers. As shown in previous cardiac tissue histology studies [2, 3], the myofiber morphology has been considered as multiple myocyte arrangements separated by extensive planes. The orientations of pig cardiac myofibers are imaged using the high frequency ultrasound imaging system, which are shown as the bright regions in Figure 4. The orientations of the bright regions in the ultrasound image Figure 4(a) are similar to the myofiber orientations in the histology image as shown in Figure 4(b) and its amplified image in Figure 4(c).

Figure 5 and 6 show the results of myofiber images of pig hearts. These images were acquired with 25-MHz and 40-MHz frequency linear probes, respectively. As shown in Figure 5(a) and 6(a), the bright fiber shapes in the ultrasound images indicate the myofiber orientations. However, the images also show bright speckles spreads that can affect the extraction results. After NLADF processing, the speckle noises in both images were reduced as shown in Figure 5(b) and 6(b). Canny edge detector and Hough transform were able to extract the edges and directions of myofibers indicated in Figure 5(c-d) and 6(c-d), respectively. After both process, the K-means clustering classified the fiber directions into 12 classes (Figure 5(e) and 6(e)) and the final results are presented in Figure 5(f) and 6(f).
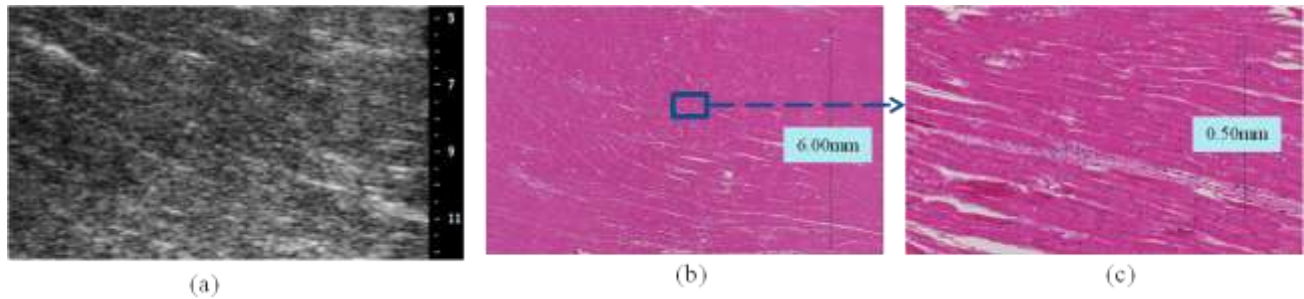
Figure 4. Myofiber orientations in high frequency ultrasound image and corresponding histologic images. (a) The ultrasound image. (b) The histologic image of the same tissue. The scale is the same as that in (a). (c) The histology image of a small region from (b) with the 10-time scale.
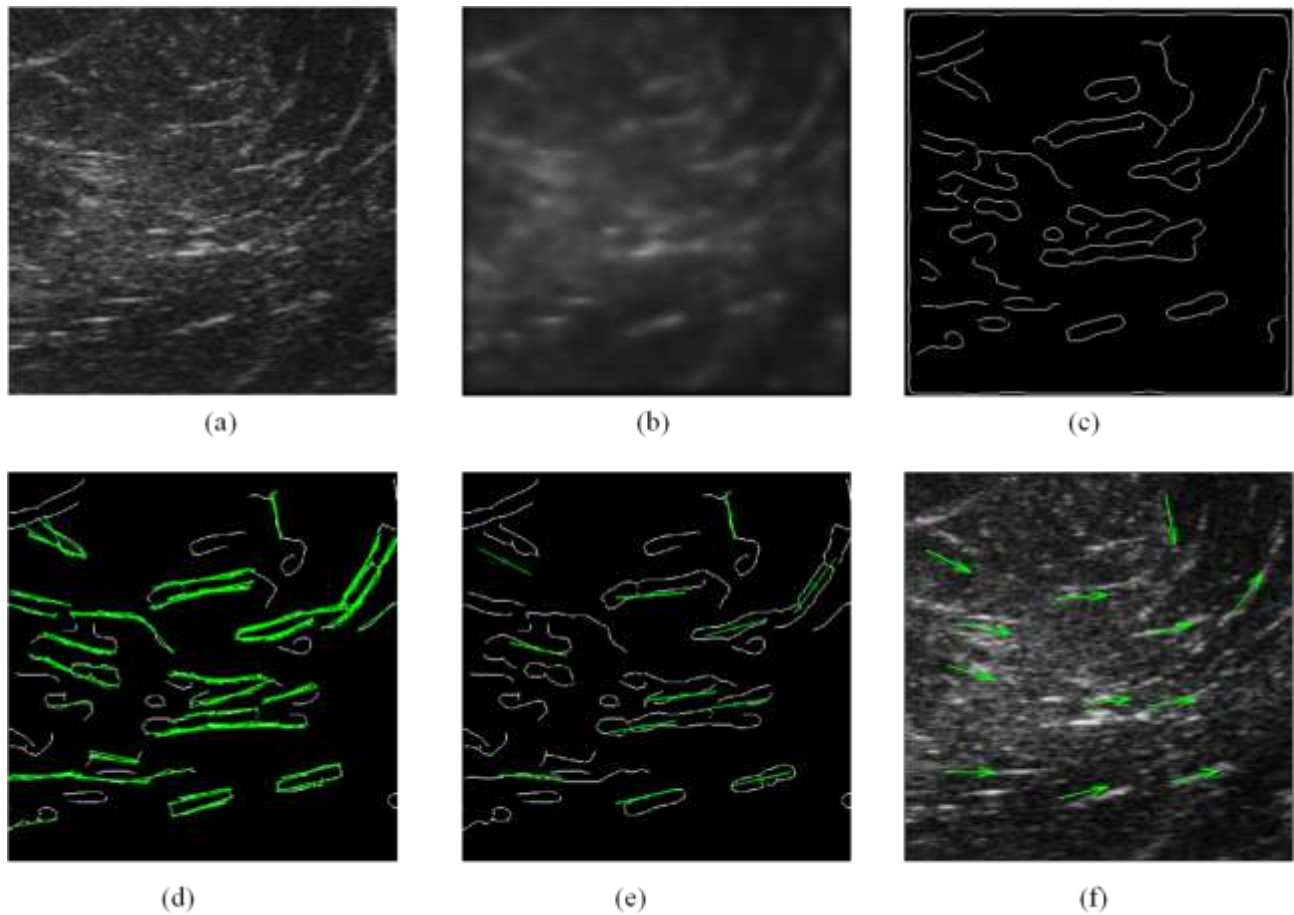

Figure 5. The extracted myofiber orientations at the heart apex from a 25-MHz ultrasound image. (a) The ultrasound image. (b) The denoising result of nonlinear anisotropic diffusion filter. (c) The edge detection result. (d) The myofiber directions detected by Hough transform (shown in green). (e) The myofiber orientations localized by K-means clustering (shown in green), where the green circles are the center points of each class. (f) The final cardiac myofiber orientations (shown in green arrows).
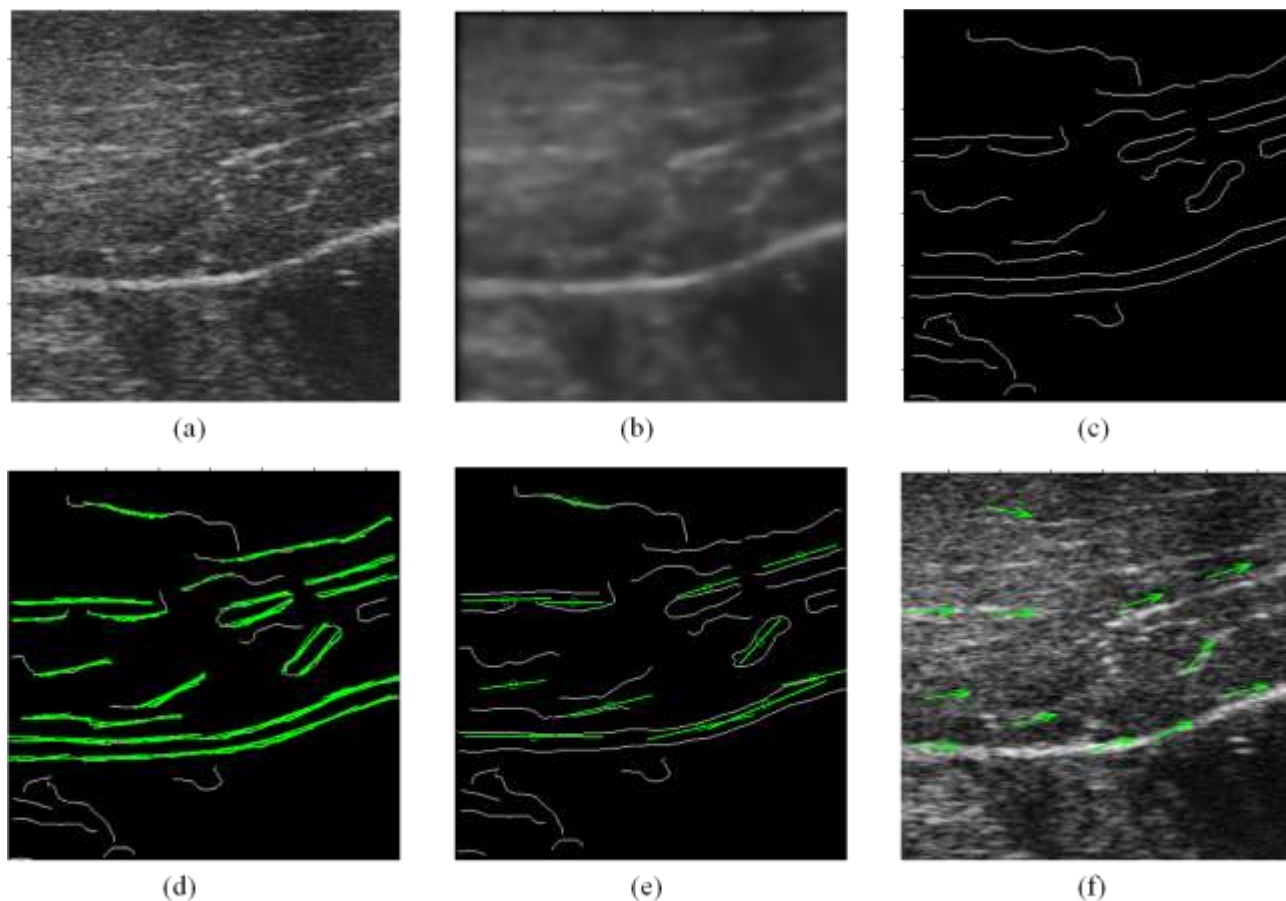
Figure 6. The extracted myofiber orientations of right ventricle from a 40-MHz ultrasound image. (a) The ultrasound image. (b) The denoising result. (c) The edge detection result. (d) The myofiber directions (shown in green). (e) The localized myofiber orientations (shown in green). (f) The final myofiber orientations (shown in green arrows).

4. CONCLUSIONS

We proposed an automatic method to extract the orientation of cardiac myofibers on high-frequency ultrasound images. To the best of our knowledge, this is the first pilot study to use high frequency ultrasound probes for cardiac fiber orientation imaging. An automatic image processing method including nonlinear anisotropic diffusion filtering was developed to extract these myofiber orientations. The proposed high frequency ultrasound imaging for cardiac fibers can have important insight for quantitative analysis of physiological and pathological functions of the heart. The results from both phantom and pig hearts showed that this method could extract myofiber orientations from the high frequency ultrasound images.

ACKNOWLEDGEMENT

REFERENCES

[1] T. Arts, F. W. Prinzen, L. H. Snoeckx et al., "Adaptation of cardiac structure by mechanical feedback in the environment of the cell: a model study," Biophysical Journal 66(4), 953-61 (1994).
[2] M. McLean, and J. Prothero, "Myofiber orientation in the weanling mouse heart," Am J Anat 192(4), 425-41 (1991).

[3] E. K. Theofilogiannakos, G. K. Theofilogiannakos, A. Anogelanaki et al., "A Fiber Orientation Model of the Human Heart Using Classical Histological Methods, Magnetic Resonance Imaging and Interpolation Techniques," Computers in Cardiology 2008, Vols 1 and 2, 307-310 (2008).

[4] L. Geerts-Ossevoort, P. Bovendeerd, F. Prinzen et al., "Myofiber orientation in the normal and infarcted heart, assessed with MR-diffusion tensor imaging," Computers in Cardiology 2001, Vol 28, 28, 621-624 (2001).

[5] L. Geerts, P. Bovendeerd, K. Nicolay et al., "Characterization of the normal cardiac myofiber field in goat measured with MR-diffusion tensor imaging," Am J Physiol Heart Circ Physiol 283, H139-45 (2002).

[6] M. T. Wu, W. Y. I. Tseng, M. Y. M. Su et al., "Diffusion tensor magnetic resonance imaging mapping the fiber architecture remodeling in human myocardium after infarction - Correlation with viability and wall motion," Circulation 114(10), 1036-1045 (2006).

[7] S. A. Wickline, E. D. Verdonk, and J. G. Miller, "Three-dimensional characterization of human ventricular myofiber architecture by ultrasonic backscatter," J Clin Invest 88(2), 438-46 (1991).

[8] M. R. Holland, A. Kovacs, S. H. Posdamer et al., "Anisotropy of apparent backscatter in the short-axis view of mouse hearts," Ultrasound in Medicine and Biology 31(12), 1623-1629 (2005).

[9] J. Crosby, T. Hergum, E. W. Remme et al., "The effect of including myocardial anisotropy in simulated ultrasound images of the heart," IEEE Trans Ultrason Ferroelectr Freq Control 56(2), 326-33 (2009).

[10] W. N. Lee, B. Larrat, M. Pernot et al., "Ultrasound elastic tensor imaging: comparison with MR diffusion tensor imaging in the myocardium," Physics in Medicine and Biology 57(16), 5075 (2012).

[11] W. N. Lee, M. Pernot, M. Couade et al., "Mapping Myocardial Fiber Orientation Using Echocardiography-Based Shear Wave Imaging," Ieee Transactions on Medical Imaging 31(3), 554-562 (2012).

[12] P. Perona, and J. Malik, "Scale-Space and Edge-Detection Using Anisotropic Diffusion," Ieee Transactions on Pattern Analysis and Machine Intelligence 12(7), 629-639 (1990).

[13] G. Gerig, O. Kubler, R. Kikinis et al., "Nonlinear Anisotropic Filtering of Mri Data," Ieee Transactions on Medical Imaging 11(2), 221-232 (1992).

[14] H. S. Wang, and B. W. Fei, "A modified fuzzy C-means classification method using a multiscale diffusion filtering scheme," Medical Image Analysis 13(2), 193-202 (2009).

[15] Y. J. Zhou, and Y. P. Zheng, "Estimation of muscle fiber orientation in ultrasound images using revoting Hough transform (RVHT)," Ultrasound in Medicine and Biology 34(9), 1474-1481 (2008).

[16] X. Yang, S. Wu, I. Sechopoulos, B.W. Fei, "Cupping artifact correction and automated classification for high-resolution dedicated breast CT images," Medical Physics 39(10), 6397-406 (2012).

[17] X. Yang, I. Sechopoulos, and B. W. Fei, "Automatic tissue classification for high-resolution breast CT images based on bilateral filtering," Proceedings of SPIE, 7962, 79623H (2011).

[18] D. MacKay, "Information Theory," Inference and Learning Algorithms, Cambridge University Press, 284–292 (2003).

[19] X. Chen, R.C. Gilkeson, B.W. Fei, "Automatic 3D-to-2D registration for CT and dual-energy digital radiography for calcification detection," Medical Physics 34, 4934-4943 (2007)

[20] H. Wang, B.W. Fei. "A modified fuzzy C-means classification method using a multiscale diffusion filtering scheme," Medical Image Analysis13, 193-202 (2009)

[21] X. Yang, B.W. Fei. "An MR brain classification method based on multiscale and multiblock fuzzy C-means," Medical Physics 38, 2879-2891 (2011)

[22] H. Wang, B.W. Fei. "An MR image-guided, voxel-based partialvolume correction method for PET images," Medical Physics, 39, 179-195 (2012).

[23] B.W. Fei, X. Yang, J.A. Nye, et al, "MR/PET quantification tools: Registration, segmentation, classification, and MR-based attenuation correction," Medical Physics 39(10), 6443-6454 (2012)

[24] H. Akbari, B.W. Fei. "3D ultrasound image segmentation using wavelet support vector machines," Medical Physics 39, 2972-2984 (2012)

[25] H. Akbari, L.V. HaligL D.M. Schuster, A. Osunkoya, V.A. Master, P.T. Nieh, G.Z. Chen, F.W. Fei. "Hyperspectral imaging and quantitative analysis for prostate cancer detection," Journal of Biomedical Optics 17, 076005 (2012)

[26] Mafi JN, Fei BW(corresponding author), Roble S, et al. "Assessment of coronary artery calcium using dual-energy subtraction digital radiography," Journal of Digital Imaging 25,129-136 (2012)

Xulei Qin ; Zhibin Cong ; Rong Jiang ; Ming Shen ; Mary B. Wagner ; Paul Kirshbom and Baowei Fei